Long Lifetime of Hydrogen-Bonded DNA Basepairs by Force Spectroscopy

Alexander Fuhrmann,[†] Sebastian Getfert,[¶] Qiang Fu,[‡§] Peter Reimann,[¶] Stuart Lindsay,[†‡§] and Robert Ros[†*]

[†]Department of Physics, [‡]Biodesign Institute, and [§]Department of Chemistry and Biochemistry, Arizona State University, Tempe, Arizona; and [¶]Condensed Matter Theory, Physics Department, Bielefeld University, Bielefeld, Germany

ABSTRACT Electron-tunneling data suggest that a noncovalently-bonded complex of three molecules, two recognition molecules that present hydrogen-bond donor and acceptor sites via a carboxamide group, and a DNA base, remains bound for seconds. This is surprising, given that imino-proton exchange rates show that basepairs in a DNA double helix open on millisecond timescales. The long lifetime of the three-molecule complex was confirmed using force spectroscopy, but measurements on DNA basepairs are required to establish a comparison with the proton-exchange data. Here, we report on a dynamic force spectroscopy study of complexes between the bases adenine and thymine (A-T, two-hydrogen bonds) and 2-aminoadenine and thymine (2AA-T, three-hydrogen bonds). Bases were tethered to an AFM probe and mica substrate via long, covalently linked polymer tethers. Data for bond-survival probability versus force and the rupture-force distributions were well fitted by the Bell model. The resulting lifetime of the complexes at zero pulling force was ~2 s for two-hydrogen bonds (A-T) and ~4 s for three-hydrogen bonds (2AA-T). Thus, DNA basepairs in an AFM pulling experiment remain bonded for long times, even without the stabilizing influence of base-stacking in a double helix. This result suggests that the pathways for opening, and perhaps the open states themselves, are very different in the AFM and proton-exchange measurements.

INTRODUCTION

The lifetime of hydrogen-bonded DNA basepairs is difficult to measure. Association constants can be measured by NMR titration (1), but these data are for organic solvents only and give no insight into the barriers that control the dissociation kinetics. [1]H studies of imino-proton exchange rates are assumed to follow base opening rates, at least in the limit of infinite concentration of the catalyst that transfers the proton in the open state (2). Based on experiments like these, G-C basepairs open on timescales of tens of milliseconds (3), whereas A-T basepairs open on timescales of milliseconds (unless incorporated into A-T tracts) (4). It seems reasonable to suppose that the motion really is an opening of the bases, because it is sensitive to the total number of hydrogen bonds, as evidenced by studies on mismatched basepairs (5).

In principle, the opening phenomenon could be studied by pulling a basepair apart with an atomic force microscope (AFM) and extrapolating data to zero applied force to discover the intrinsic thermal dissociation rate. The forces that hold bases together in an oligomer have been measured (6–8) with a resolution down to a single base (9), but kinetic data have not been reported. This article reports a study of the dissociation kinetics of DNA basepairs using dynamic force spectroscopy (DFS).

At the outset, one might expect that the lifetime of an isolated hydrogen-bonded basepair would be much less than that of a basepair inside a double helix, because of the influ-

ence of stacking forces (9,10). However, bursts of tunneling signal from individual bases trapped in a tunnel junction consisting of two gold electrodes, separated by a gap of ~2.5 nm and each functionalized with mercaptobenzamide molecules, appeared to last for seconds, implying that the DNA bases were trapped for a long time in a noncovalently-bonded complex with the mercaptobenzamide molecules (11). We used DFS to study a complex formed between benzamide molecules on the surface and probe (tethered by polyethyleneglycol (PEG) polymers) and adenosinemonophosphate, finding that the complex remained bound for about 3 s at zero force (11). Here, we report on a study of the A-T basepair and its triply hydrogen-bonded analog, 2AA-T. The lifetime of the bound pair at zero applied force is found to be seconds also.

AFM-based DFS is widely used to investigate molecular recognition on the single-molecule level (e.g., reviewed in Zlatanova et al. (12) and Fuhrmann and Ros (13)). The binding partners of interest are attached to the AFM tip and a surface via well-characterized PEG tethers (see Fig. 1 A) and the probe displacement, s, can be controlled with nanometer precision. The force, $F(s)$, acting on the tip is measured as a function of the distance, s, while the tip is cycled up and down relative to the surface. Retracting the probe with constant speed $v = \dot{s}(t)$ increases the force acting on the chemical bond between the two binding partners until the molecules dissociate. In DFS, the distribution of the rupture forces is measured for various speeds of retraction. Quantitative information about the energy-landscape parameters and kinetic constants of the interaction can be obtained from these experiments (14).

We show that after careful preprocessing, our DNA basepair data are consistent with the assumption that forced

---

Alexander Fuhrmann's present address is Department of Bioengineering, University of California, San Diego, La Jolla, CA.
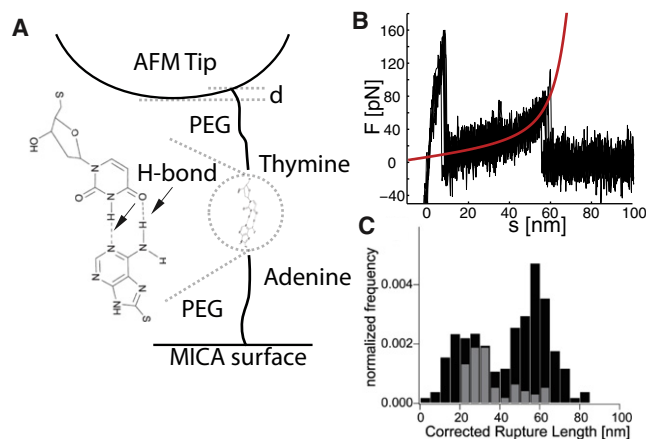
Editor: Peter Hinterdorfer.

FIGURE 1 (*A*) DNA bases thymine (T) and adenine (A) or 2-aminoadenine (2AA) are immobilized via ~30-nm-long PEG linkers on the AFM tip and sample surface, respectively. The offset, *d*, indicates that the attachment point of the linker molecule is randomly distributed. (*B*) Overlay of nine representative force-extension curves measured between 2AA and T at 2000 nm/s pulling speed. The solid line shows the result of an FJC fit according to Eq. 2. (*C*) Normalized rupture length of the T-2AA interaction (*black/background*) and 2AA-2AA (*gray/foreground*) as control at a pulling speed of 2000 nm/s.

bond rupture can be modeled as a one-step rate process. We estimate the lifetimes of the complexes and energy-landscape parameters employing different functional forms of the force-dependent dissociation rate. We finally show that if the rupture-force data are preprocessed less strictly, some unusually high rupture forces contribute to the rupture-force distribution. These forces can likely be attributed to the almost synchronous rupture of multiple parallel bonds, which remains undetected by previous standard data-selection criteria. We extend a recently proposed model (15) that accounts for multiple bonds and apply it to our data, yielding rate parameters very similar to those obtained for the more strictly preprocessed data.

MATERIALS AND METHODS

AFM tip and surface modification

Si$_3$N$_4$ cantilevers (MSCT, Veeco, CA) were first dipped in concentrated nitric acid for ~3 s for activation and then rinsed with water and ethanol. After drying with argon, the cantilevers were silanized with aminopropyl-triethoxysilane in a desiccator together with freshly cleaved mica. The tips, as well as the mica, were incubated in a linker solution of 0.2 μmol/l maleimide PEG succinimidyl valerate (MAL-PEG- SVA, molecular mass 3.4 kD; Laysan Bio, Arab, AL) and 2 μmol/l methoxy PEG succinimidyl valerate (mPEG-SVA; molecular mass 2 kD; Laysan Bio) in chloroform for 2 h. The samples were then dipped into chloroform. Then, 0.85 mg of 5′-mercaptothymidine (T) (16) was dissolved in 5 ml methanol, resulting in a 1 mM solution. Four drops of pyrrolidine were added to deacetylate the thiol tag, and 3.64 mg of 2-amino-8-mercapto-adenine (2AA) or 8-mer-capto-adenine (A) (Aldrich, St. Louis, MO) was dissolved in 20 ml dime-thylformamide, resulting in a 1 mM solution. All solutions were then further diluted 100 times to give 10 μM. The tips were then functionalized with T and the substrates with 2AA or A, respectively. A drop of water was added to ensure binding of the bases to the linkers. After 2 h, the cantilevers

and samples were rinsed with chloroform, ethanol, and finally water. Measurements were then performed in phosphate-buffered saline and also, for control purposes, in water.

Force spectroscopy experiments

An MFP-3D (Asylum Research, Santa Barbara, CA) was used. The calibration of the cantilevers and all force spectroscopy experiments were done with the provided software based on Igor Pro (Wavemetrics, Lake Oswego, OR), yielding spring constants of 50–60 pN/nm. Force-extension curves were taken using a constant approach speed of 5000 nm/s, a trigger point of 600 pN, and a dwell time of 0.2 s. The retract speed was varied between 100 and 5000 nm/s. The force-curve analysis was done using custom-written software in Igor Pro, as described previously (17). Model parameters and statistical errors were estimated using the maximum-likelihood method (18).

Simulations of force-distance curves

The basic idea of the multiple-bond model (see Figs. 5 *B* and 6 *B*) is outlined in the section Multiple rupture events. The force acting on a single bond is determined by the full configuration of the complex of all intact bonds. For the simulation of the force-extension curves in Fig. 5 *B*, we dropped the assumption of the simultaneous rupture of all bonds and employed a Monte Carlo scheme. The rupture of each single bond was modeled by a one-step rate process and the force-dependent dissociation rate was approximated by Eq. 1. with $\gamma = 1$. For a better comparison to experimental force-extension curves, we added a Gaussian noise to the simulated curves. Further details are given in the Supporting Material.

THEORETICAL BACKGROUND

The theoretical modeling of single-bond rupture in DFS is well established (see, e.g., (14,19–21)). In brief, the rupture of a bond that is subjected to a time-dependent force, $F(t) = F(s(t))$, is a one-step rate process with the force-dependent dissociation rate $k(f)$. The exact functional dependence of $k(f)$ on force f is determined by the underlying reaction potential, $U(x)$, where x denotes the reaction coordinate. Many models describing this dependence have been developed (14,21,22) and it has been shown that for various such models the dissociation rate can be written in the form (19)

$$k(f) = k_0 \left(1 - \frac{\gamma \alpha f}{\varepsilon}\right)^{\frac{1}{\gamma}-1} \exp\left[\varepsilon\left(1 - \left(1 - \frac{\gamma \alpha f}{\varepsilon}\right)^{\frac{1}{\gamma}}\right)\right]. \quad (1)$$

The three model parameters are k_0, α, and ε, and they have the following physical meanings: k_0 is the force-free dissociation rate; $\alpha = x_b/k_BT$ denotes the distance x_b from the minimum of the reaction potential to the barrier divided by the thermal energy, k_BT, where k_B is Boltzmanns constant and T is the temperature; and $\varepsilon = \Delta U/k_BT$ stands for the force-free activation energy barrier, ΔU, in units of thermal energy. The extra parameter γ usually takes one of the three values $\gamma = 1/2$, $\gamma = 2/3$, and $\gamma = 1$, corresponding to a parabolic potential well with a cusp barrier, a cubic reaction potential, and a piecewise linear potential, respectively. In the latter case, $\gamma = 1$, parameter ε drops out and one recovers Bell's model (14,23).

The probe displacement, $s = vt$, can be written as the sum of the extension of the PEG linkers and the deflection of the cantilever under the instantaneously applied force. The former can adequately be described by a modified freely jointed chain (FJC) model (24), resulting in the following transcendental equation for the force-extension curve, $F(s)$, which can be easily solved numerically:

$$s = \frac{F(s)}{\kappa} + L\left[\coth\left(\frac{F(s)L_K}{k_B T}\right) - \frac{k_B T}{F(s)L_K}\right] - d. \quad (2)$$

Here, κ is the spring constant of the AFM cantilever, L the sum of the two contour lengths of the linkers, L_K the Kuhn length, and d the offset between cantilever tip and attachment point of the linker (see Fig. 1 A).

For a given force dependence of the dissociation rate, $k(f)$, and a given force-extension curve, $F(s)$, the survival probability of the bond up to force f is (14)

$$n(f) = \exp\left[-\frac{1}{v}\int_{f_0}^{f} df' \frac{k(f')}{F'(F^{-1}(f'))}\right], \quad (3)$$

where $F'(s)$ denotes the derivative of the function $F(s)$ with respect to probe displacement s, $F^{-1}(s)$ the concomittant inverse of $F(s)$, $f_0 = F(s = 0)$, and $v = \dot{s}$ the retraction speed. Hence, the probability density of rupture forces follows as $p(f) = -dn(f)/df$. Closer inspection of Eq. 3 shows that the function $-v\ln n(f)$ should not depend on the retraction speed (25,26) independent of the exact functional form of $k(f)$ and $F(s)$ and therefore provides a method to experimentally check whether or not the DFS data are compatible with the one-step reaction kinetics assumed in Eq. 3. Raible et al. (26) have performed this consistency check for various data sets measured by either AFM or the biomembrane force probe. The astonishing result was that the $-v\ln n(f)$ plots were not independent of pulling velocity for any of these data sets (or for any other DFS data set on receptor-ligand systems that the authors know of). In all cases, the curves depended on pulling velocity in a very similar way (11,17,20,26–28).

RESULTS AND DISCUSSION

Dissociation forces for AA-T and A-T

To investigate the lifetime of hydrogen bonds under external force load, we immobilized thymine (T) via ~30-nm-long PEG linkers covalently to the AFM tip. On the mica surface, we immobilized 2-amino-adenine (2AA) or adenine (A) via the same ~30-nm-long PEG linkers (Fig. 1 A). 2AA can form three hydrogen bonds with T, instead of the two of A-T. A polymer linker is widely used to exclude unspecific interactions between the tip and the surface and forces due to the dissociation of multiple complexes (29,30). Here, we used PEG linker molecules on the tip and the surface.

To control the surface coverage, we used a mixture of PEG linkers, one with functional groups for the attachment of thiol-modified bases and the other lacking these maleimide groups, at a ratio of 1:10. In AFM-DFS experiments, the functionalized AFM tip is moved toward the sample surface and then retracted while the force acting on the cantilever is recorded. During the retracting part of the cycle, the dissociation of the complex can be identified as a discontinuity at a distance corresponding approximately to the length of the elongated linker molecules. Fig. 1 B shows the overlay of nine retraction curves for T-2AA interactions at a pulling speed of $v = 2000$ nm/s. All curves show unspecific adhesion between the tip and the surface of ~160 pN for tip retractions <10 nm. After this adhesion peak, the curves show the stretching of the linker molecules and dissociation of the complexes at ~60 nm. For a quantitative evaluation of the DFS data, an adequately parameterized approximation of these curves is needed (see Eq. 3). The solid line in Fig. 1 B represents the least-squares fit of Eq. 2 to the measured retraction curves. We used the experimentally determined value $\kappa = 50$ pN/nm for the cantilever stiffness, with the contour length, L, the Kuhn length, L_K, and the offset, d (see Fig. 1 A), as adjustable parameters. The best-fit values are found to be $L = 83.7$ nm, $L_K = 0.39$ nm, and $d = 15.1$ nm. As can be seen in Fig. 1 B, the FJC model with these parameters describes the force-extension characteristics very well in the force regime dominant in this experimental series (<100 pN). Further corrections or modifications to the model (e.g., Oesterhelt et al. (31) and Sulchek et al. (32) are not necessary. It is worth noting that there are other combinations of parameters that fit the data almost equally well, and employing those modified models would additionally yield slightly different parameter values. Hence, it is not surprising that the fitted parameters slightly deviate from the expected values. In particular, the contour length is larger than the expected length, $L_{th} \approx 60$ nm, and the attachment point of the linker ($d = 15.1$ nm) is quite large compared to the equilibrium radii of gyration of free polymers. Concerning the latter observation, the large fitted value of d appears unlikely and also explains why the fitted L is considerably larger than L_{th}. However, we remark that the formation of bonds between two molecules is a nonequilibrium process that is additionally subjected to very complicated boundary conditions, and hence, offsets $d \approx 15$ nm cannot be ruled out. As an experimental estimate of the FJC parameters is not the purpose of this article, we confine ourselves to the observation that the quantitative evaluation of the righthand side of Eq. 3 in the following analysis just requires a good approximation of the force-extension curve, $F(s)$, which (in view of Fig. 1 B) is provided by Eq. 2 supplemented with the fitted FJC parameters.

The black bars in Fig. 1 C show the distribution of the rupture length of the T-2AA interaction at a pulling speed of 2000 nm/s. The histogram shows a bimodal distribution

with maxima at ~30 nm and ~60 nm. The total rupture probability is 5.3%, as the molecule density is kept sparse to decrease multiple rupture events (the total rupture probability of all experimental data is between 3% and 6% for 2AA-T and between 5% and 11% for A-T). As a control experiment, we used AFM tips functionalized with 2AA instead of T. The resulting histogram (Fig. 1 C, gray) shows one major peak at ~30 nm at a rupture probability of 0.8%, indicating that the peak at 60 nm in the former distribution belongs to the hydrogen-bond-based 2AA-T interaction. The peak at 30 nm is the result of direct interactions between the AFM tip surface and the polymers on the surface or between the polymers on the tip and the surface. This shows the importance of using two long linker molecules, since unspecific linker-surface interactions are always present. In what follows, only rupture curves corresponding to two linkers will be accepted (see below); ~35% of the events were not used for further processing, as they were too short.

Here, we describe briefly the exclusion of unspecific and multiple rupture events (a detailed description of the data analysis is given in Fuhrmann et al. (17)). First of all, unspecific events are filtered out by allowing only rupture forces corresponding to the combined length of the two linker molecules. This length is ~60 nm (two 30-nm PEG linkers) for a fully stretched pair. Due to linker-length variations and different attachment points on the round AFM tip, we considered a variation of ~8 nm (distance d in Fig. 1 A). However, at lower pulling velocities, the bonds between the two bases break before the linker molecules are fully stretched. We accounted for this in the analysis by decreasing the accepted rupture lengths to 35 nm for low pulling velocities and low rupture forces. We applied three additional criteria (17) to exclude force data from multiple rupture events arising from the simultaneous pulling on more than one molecular pair. First, only rupture curves beginning monotonically below a certain threshold, f_{min}, were accepted. The parameter f_{min} is usually chosen to be slightly higher than the noise strength. For the analysis, we used $f_{min} = 10$ pN for pulling speeds ≤ 1000 nm/s and $f_{min} = 20$ pN for pulling speeds >1000 nm/s. To determine whether a rupture curve meets those requirements we fitted a second-degree polynomial from the point of rupture backward to the baseline (17). If the polynomial fit notably deviated from the force curve before reaching this f_{min}, the curve was rejected. The second criterion requires that the cantilever jump immediately back to the baseline after a rupture event. Third, we constructed a master curve by averaging over all polynomial fits. Measurements showing large deviations from this master curve were identified and excluded from the evaluation. However, this last criterion did not further improve the quality of the data (i.e., narrowing the force distribution) and was subsequently not used for the main analysis. This filtering resulted in a further reduction of accepted rupture events. For A-T, 50 ± 6% (mean ± SD) of the rupture curves meeting the minimum rupture length

criterion were accepted, and for 2AA-T, this value was 52 ± 15%. Applying all filters, the total accepted rupture probability was between 2% and 4% for A-T bonds and between 1% and 2% for 2AA-T bonds. Having a total rupture probability of <11% but a multiple rupture probability of ~50% clearly indicates that our efforts to prevent linker clustering (see Materials and Methods) were not as efficient as intended. Although the multiple rupture events did not affect the quality of the data (our software was able to detect and filter them), subsequent works should seek to improve linker-length dispersity, as this is important for the general field of single-molecule force spectroscopy.

For the DFS experiments, we probed both samples (A and 2AA) with different pulling speeds. Fig. 2, A and B, shows rupture-force histograms of the A-T and 2AA-T interactions at retraction speeds of 100 and 500 nm/s, respectively. For the experiments, the same cantilever modified with T was used to eliminate errors in cantilever spring constant calibration. For both pulling speeds, the 2AA-T rupture forces are higher compared to the A-T, showing that the two- and three-hydrogen- bonded cases yield different rupture forces. The distributions have maxima at 20 pN (T-A) and 31 pN (T-2AA) at 100 nm/s. For 500 nm/s, we found values of 29 pN for T-A and 44 pN for T-2AA.

There have been several approaches to measure unbinding forces for DNA bases and nucleotides in the literature using DFS (8,9,33,34). These experiments reveal that base stacking of DNA has a much higher contribution to the strength of a DNA double helix than the individual bonds between the nucleotides. However, due to the experimental setup, these molecules are nearly always pulled apart with a force applied at an angle to the bond direction or under shear stress. Gaub et al. were able to unzip double-stranded DNA nucleotide by nucleotide (35). The measured forces to unzip the basepairs are, depending on the sequence, between 10 and 20 pN. Diezemann and Janshoff (36) investigated reversible bond breaking by means of Brownian dynamics simulations. Typical hydrogen-bond rupture forces of ~40 pN and ~70 pN were calculated for loading rates of 300 pN/s and 30,000 pN/s, respectively. The simulated linkers were very stiff and short. Vancso et al. (37,38) have measured the rupture forces of quadruply
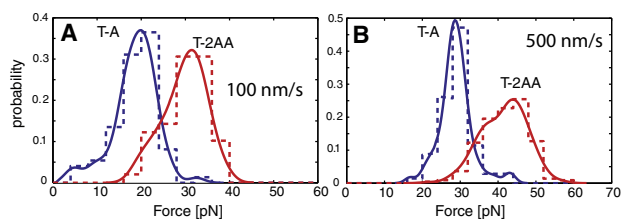

FIGURE 2 Kernel density estimators (solid lines) and histograms (dashed lines; 4-pN binning) of the rupture forces of the two different binding mechanisms at pulling speeds of 100 nm/s (A) and 500 nm/s (B). The same cantilever was used for all measurements in A and B. Each distribution is normalized to the total number of rupture events.

H-bonded dimers. Using short linkers resulted in rupture forces between 150 and 250 pN, roughly consistent with the data we report here for two- and three-hydrogen bonds.

Lifetimes and binding potentials of the complexes

Figs. 3 and 4 show the experimental rupture-force distributions of the 2AA-T and A-T complexes for different retraction speeds. For a given retraction speed, the survival probability, $n(f)$, can be approximated by the fraction of rupture forces that are larger than f. Doing this for each retraction velocity, we have plotted the functions, $-v\ln n(f)$, against the forces, f. We found for both the 2AA-T and the A-T interactions (Figs. 3 A and 4 A) that these functions collapse almost perfectly onto a single velocity-independent curve. This is a requirement for the application of the theoretical models, which are based on a one-step rate process. Such models are used for the quantitative evaluation of the majority of DFS studies, although this basic requirement is in general not met (see Theoretical Background). To our

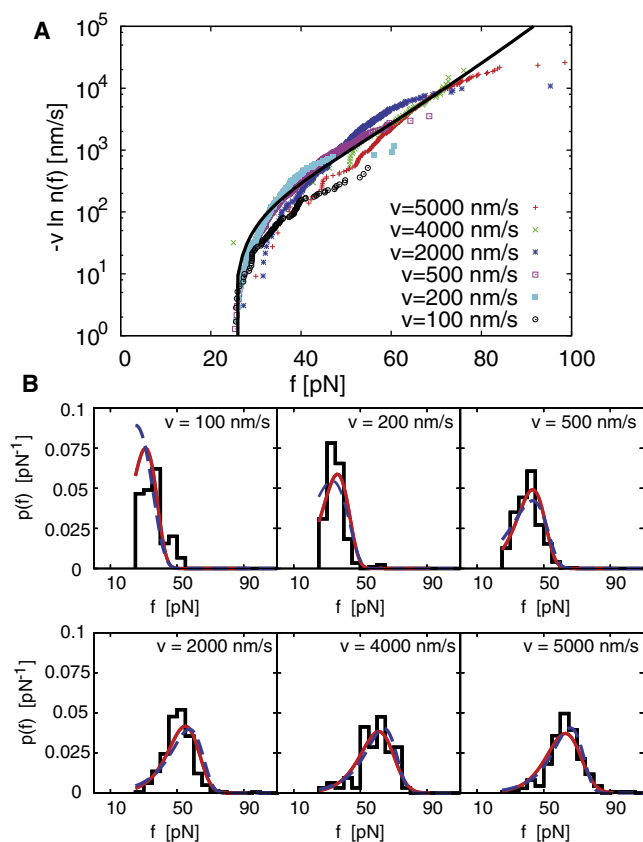knowledge, this is the first DFS data set for complex dissociation showing the collapse of the $-v\ln n(f)$ functions, and thus the first rupture data set that is in full agreement with the usual theoretical models. In the following, we employ a maximum-likelihood estimator to estimate the rate parameters, which enter into the model via Eq. 1, for the different values of the exponent γ.

Figs. 3 B and 4 B show the rupture-force data plotted as histograms. The dashed blue lines are maximum-likelihood fits for the classical Bell model (Eq. 1) with exponent $\gamma = 1$. The same fits are shown in Figs. 3 A and 4 A by the black solid lines. For the 2AA-T interaction (Fig. 3) we estimated a thermal dissociation rate of $k_0 = 0.23 \pm 0.02$ s^{-1} which corresponds to a lifetime of the complex of 4.4 ± 0.4 s. This is comparable to the lifetime measured for the complex of two benzamide molecules with AMP (11). For the A-T interaction with two hydrogen bonds involved, the standard Bell model yields $k_0 = 0.52 \pm 0.07$ s^{-1} (i.e., a lifetime of 1.9 ± 0.3 s). Hence, the additional hydrogen bond increases the lifetime of the complex by a factor of ~2. The estimate for the remaining parameter of the Bell model, the distance of the potential minimum from the barrier, is 0.6 ± 0.01 nm ($\alpha = 0.142 \pm 0.002$ pN^{-1}) for the 2AA-T complex and 0.7 ± 0.02 nm ($\alpha = 0.172 \pm 0.004$ pN^{-1}) for the A-T complex. These values are larger than expected for a hydrogen-bonded interaction and may indicate that base stacking interactions play an additional role. Because the functional form of the reaction potential of the basepair interaction is unknown, it is a priori not clear which exponent γ in Eq. 1 results in the most appropriate approximation for the force dependence of the reaction rate. We have therefore also fitted the rupture force data for the other two commonly employed exponents, $\gamma = 2/3$ (i.e., a cubic reaction potential) and $\gamma = 1/2$ (i.e., a parabolic potential with a cusp barrier). The maximum-likelihood estimates for the model parameters are listed in Table 1 and the fitted distributions for $\gamma = 2/3$ are shown in Figs. 3 B and 4 B by

TABLE 1   Dissociation-rate parameters and their statistical uncertainties for 2AA-T and A-T bonds

	2AA-T			A-T		
	$\gamma = 1$	$\gamma = 2/3$	$\gamma = 1/2$	$\gamma = 1$	$\gamma = 2/3$	$\gamma = 1/2$
k_0 (s^{-1})	0.23	0.030	0.015	0.52	0.18	0.17
Δk_0 (s^{-1})	0.02	0.006	0.004	0.07	0.05	0.06
Lifetime (s)	4.4	33.3	64.9	1.9	5.6	5.9
ΔLifetime (s)	0.4	7.0	18.2	0.3	1.6	1.9
α (pN^{-1})	0.142	0.227	0.264	0.172	0.237	0.243
$\Delta\alpha$ (pN^{-1})	0.002	0.008	0.012	0.004	0.016	0.021
ε (k_BT)	—	14.37	16.21	—	13.97	17.38
$\Delta\varepsilon$ (k_BT)	—	0.26	0.27	—	1.34	2.50

FIGURE 3   (*A* and *B*) Experimental rupture-force data for the 2AA-T interaction are shown as symbols (*A*) and histograms (*B*). The survival probability, $n(f)$, in *A* was approximated by the fraction of rupture events at forces $>f$. The solid line in *A* and the dashed lines in *B* represent the maximum-likelihood fit for Bell's model (Eq. 1. with $\gamma = 1$). The corresponding fits for the exponent $\gamma = 2/3$ are shown by the solid lines in *B*. The fitted distributions for $\gamma = 1/2$ coincide with these curves within linewidth.

Parameters and their uncertainties are given for complexes with three-hydrogen (2AA-T) and two-hydrogen (A-T) bonds. $\gamma = 1/2$ corresponds to a parabolic potential well with a cusp barrier, $\gamma = 2/3$ to a cubic reaction potential, and $\gamma = 1$ to the piecewise linear potential of the standard Bell model. The statistical uncertainties were calculated according to the methods of Getfert et al. (18).

the red solid lines. Because the corresponding distributions for $\gamma = 1/2$ coincide with these lines within linewidth, they are not shown separately. Compared to the Bell model, no quantitative statement about which exponent fits the data best is possible, but, as previously observed (18,19,39,40), the quantitative values for the rate parameters differ considerably for the different exponents (see Table 1). In particular, these differences are considerably larger than the estimated statistical uncertainties of the model parameters (for a fixed model) and can therefore not be ascribed to the limited sample size (18). However, for each exponent, the lifetime of the bond lies in the range of a few seconds, and for each fixed exponent, the lifetime of the 2AA-T complex exceeds the lifetime of the A-T complex by a factor of between 2 and 10, as expected from the fact that the 2AA-T complex forms one hydrogen more than the A-T complex. Concerning the estimated height of the activation energy barrier, the fitted values lie in the range between 14 $k_B T$ and 17 $k_B T$, which appear to be reasonable values for bonds with a lifetime of a few seconds. However, the estimated values for the two different complexes did not deviate beyond expected statistical uncertainties. This can be explained by the fact that the height of the energy barrier cannot be very accurately determined by DFS and that the statistical uncertainties are often underestimated for small sample sizes (see discussion in Getfert et al. (18)).

Finally, we have also compared our parameter values with those obtained from the classical evaluation of DFS experiments (14), namely by determining the maximum f^* of the force distributions for each retraction velocity and plotting it semilogarithmically against the loading rate, which is defined as the product of the retraction velocity with the slope of the force-extension curve at the most probable rupture force, f^* (Fig. 4 B). From the slope and the extrapolation to zero force, the thermal dissociation rate, k_0, and the distance α can be determined (33). The parameters obtained in this way coincide with the maximum-likelihood estimates for $\gamma = 1$ in Table 1 within a few percent.

Multiple rupture events

All data shown so far have been preprocessed to eliminate multiple rupture events with our custom software. Comparison with other commonly used preprocessing methods is difficult, since only a few groups provide sufficient details. A widely adopted approach is to allow only so-called last rupture events (28,33,41–47). This would mean that as long as the cantilever jumps back immediately to the baseline after the rupture event, the rupture would be accepted. In addition we also applied the $f_{\min}$ criteria, requiring that the polynomial fit go from the point of rupture at least to a certain force close to the baseline (see above). Fig. 5 A shows an overlay of eight measured curves that satisfy the rupture-force value of the last peak criterion but not the $f_{\min}$ criterion. The reanalyzed data set for the A-T interaction
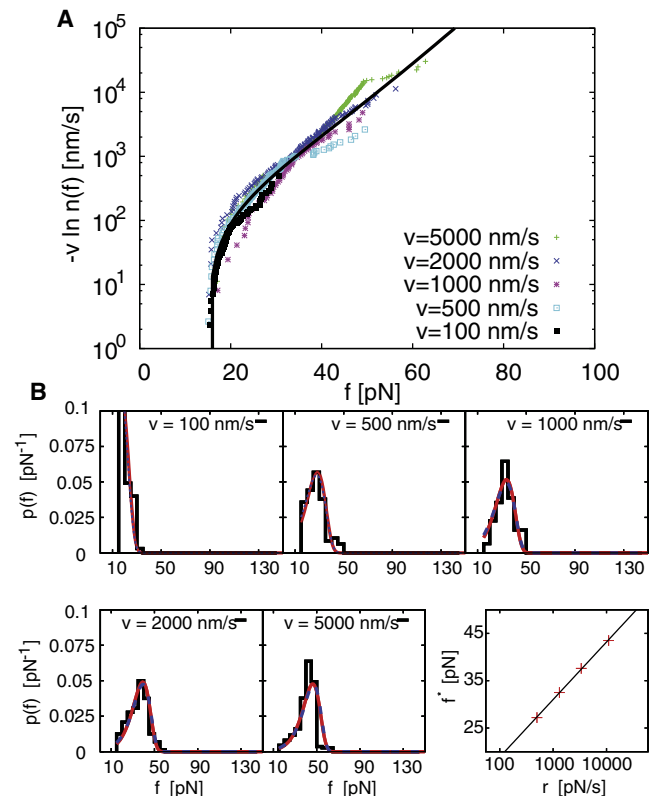
FIGURE 4 Experimental rupture-force data for the T-A interaction, similar to Fig. 3. In addition, in B, the classical semilogarithmic Bell-Evans plot (most probable rupture force, f^*, versus loading rate, r) is shown.

using this less strict selection criterion is shown in Fig. 6. It can be clearly seen that a considerable number of high rupture forces have now been accepted and that the $-v \ln n(f)$ plots now depend on the pulling velocity (Fig. 6 A). This
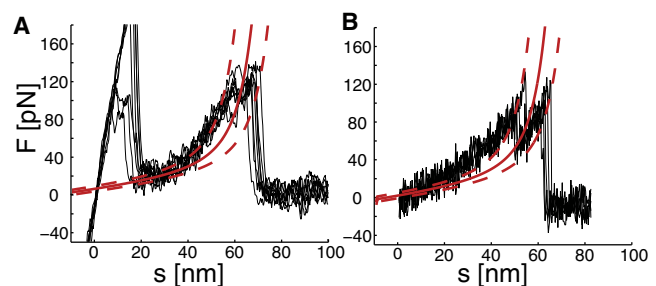

FIGURE 5 (A) Overlay of eight force-extension curves exhibiting relatively high rupture forces, experimentally observed for the T-2AA interaction at a pulling velocity of $v = 2000$ nm/s. The solid lines are the same as in Fig. 1 B. The dashed lines were obtained by shifting the solid line by 7 nm to the negative or positive. Although the experimental force-extension curves closely follow the shifted fitted curve for forces <100 pN, they considerably deviate at higher forces. (B) Eight simulated force-extension curves for a complex of three parallel bonds. For two of these bonds, the linker molecules were attached close to the tip apex, whereas the third bond had an offset of $d \approx 5$ nm. The force dependence of the dissociation rates was approximated by Bell's model with parameters from the fit to the data shown in Fig. 3. The contour length and the Kuhn length were taken from the fit to the experimental force-extension curves in Fig. 1 B.
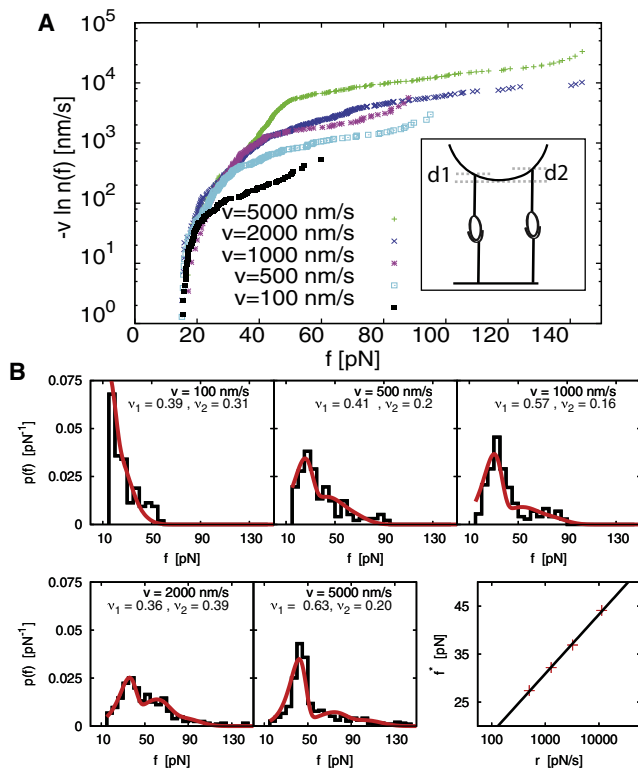
FIGURE 6 (*A*) Same data set (T-A) as in Fig. 4, but with f_{min} criteria loosened to increase the probability of multiple-rupture events. (*Inset*) Illustration of simultaneous pulling over two molecules. Note that the attachment points of the linkers are randomly distributed. The resulting distances to the end of the tip are indicated by d_1 and d_2. (*B*) The solid lines indicate the fits using the multiple-bond model, as described in detail in the main text.

0.58 s^{-1} and $\alpha = 0.187$ pN^{-1}, which are in good agreement with the values for $\gamma = 1$ in Table 1.

To further test our assumption that the high forces can be attributed to the almost synchronous (and thus undetected) rupture of multiple parallel bonds, we extended a model that was recently proposed by Guo et al. (15). Details of the model are given in the Supporting Material. In brief, we consider the situation in which one pulls on $N = 1,2,3,\dots$ parallel bonds with relative frequency ν_N. The corresponding molecules are connected to tip and sample via PEG linkers of equal length, but each linker has a different immobilization point on the cantilever tip, i.e., a different offset, d, in Eq. 2. (see Fig. 6 *A*, *inset*). Effectively, we thus also cover the case where the PEG molecules are not monodisperse. As a consequence, for a given distance between tip and surface, the linker molecules are stretched to different lengths and the force is unequally distributed among the bonds. It is further assumed that once the first bond has ruptured, the remaining bonds quickly follow (in the opposite case, the rupture events would be filtered out even with our less strict data preprocessing criterion). Hence, the survival probability of the complex is the product of the survival probabilities of the single bonds, each of which is given by an expression similar to Eq. 3. Finally, one needs to average over all possible combinations of the above-mentioned offsets, d. Employing the above-determined rate parameters ($k_0 = 0.58$ s^{-1} and $\alpha = 0.187$ pN^{-1}), assuming that $\nu_N = 0$ for $N > 3$, and noting that $\nu_3 = 1 - \nu_1 - \nu_2$, we fitted ν_1 and ν_2. The results (Fig. 6, *solid lines*) indicate the fits of the multiple-rupture model and show good agreement with the data. In particular, for the different pulling velocities, we found the probability of observing single-rupture events (ν_1) to be between 36% and 63% (the values for each pulling velocity can be found in Fig. 6 *B*). We obtained similar results for 2AA-T (Fig. S1 in the Supporting Material). The lower linker density and the thus lower rupture probability of 2AA-T increases the probability of detecting single-molecule events, which range between $\nu_1 = 58\%$ and almost 100%.

Noy et al. (32) have shown that it is possible to identify the number of linker molecules that were simultaneously pulled on. However, this only works for rupture forces >~100 pN. Akhremitchev et al. (15) analyzed the shape of multiple-rupture force-extension curves at lower rupture forces and concluded that there is a high probability of obtaining curves that appear exactly like single-molecule ones. Similar conclusions were derived in Karácsony and Akhremitchev (48) and Getfert and Reimann (49). To further validate that the occasionally observed curves, like those in Fig. 5 *A*, are results of multiple-rupture events, we simulated force-extension curves based on the standard and multiple-bond models described previously. To demonstrate the principle function of our simulation method, we reproduced the force-extension curves from Fig. 1 *B* using all fit parameters from the FJC model, a realistic noise

means that the data can no longer consistently be described within the framework of the simple theoretical models presented in the introduction. We attribute this (seeming) incompatibility with the common models to the fact that as a consequence of our less strict selection criterion, some rupture forces are now accepted that are due to the rupture of multiple parallel bonds, which are not properly accounted for by those models. There are several experimental observations that support multiple rupture events as the source of the discrepancy. 1), Many force-extension curves that result in high rupture forces display an unusual behavior at high forces. In particular, we observed in several cases small force dips or a decreasing slope of the force-extension curve at high forces (see Fig. 5 *A*). 2), Although the frequency of rupture events increases at higher forces, the pronounced main force peaks (i.e., the most probable rupture forces) do not seem to be shifted compared to those from Fig. 4 *B*. In Fig. 6 *B*, similar to Fig. 4 *B*, we estimate the rate parameters k_0 and α in the classical way on the basis of the most probable rupture forces (14). As discussed in Raible et al. (20), this dependence can be very well fitted with the usual theoretical models, even if the $-v\ln n(f)$ plots and also the rupture force distributions show significant dependence on pulling speed. The resulting parameters are $k_0 =$

strength, and the estimated force dependence of the dissociation rate within Bell's model. Except for that from the missing adhesion, which we saw no reason to include in the simulation, the simulated curves were indeed found to be nearly undistinguishable from the experimental data. In contrast, the only possible way to get force-extension curves like those shown in Fig. 5 A, with small force dips or a decreasing (average) slope at high forces, was to assume that one pulls on a complex of parallel bonds. Fig. 5 B shows a number of simulated force-extension curves for a complex of three parallel bonds. These are similar to the experimentally measured curves in Fig. 5 A. The remaining deviations might be explained by a limited experimental resolution and by the fact that our theoretical model describes only very roughly the relaxation to the new force equilibrium after rupture of a single bond.

CONCLUSION AND OUTLOOK

We found in our single-molecule force spectroscopy experiments that the lifetimes for the DNA base-complexes A-T and the modified AA-T complexes (three-hydrogen bonds) are in the range of seconds. This is surprising, given that imino-proton exchange rates show that basepairs in a DNA double helix open on millisecond timescales. Thus, DNA basepairs in an AFM pulling experiment remain bonded for long times, even without the stabilizing influence of base stacking in a double helix. We cannot exclude additional stacking-like interactions between our two bases. However, the result that the measured rupture forces and lifetimes scale with the number of hydrogen bonds suggests that the dominating factor for the interactions is indeed the hydrogen bonds. This result suggests that the pathways for opening, and perhaps the open states themselves, are very different in the AFM and proton-exchange measurements. The results also confirm lifetimes for the three-molecule complexes benzamide-nucleotide-benzamide we determined in previous single-molecule force spectroscopy and electron-tunneling experiments (11).

We note that lifetimes beyond 0.1 s immediately follow from the observed rupture forces without any further theoretical modeling; e.g., in Fig. 2 B, we see that a considerable number of T-2AA bonds only rupture beyond 40 pN and hence, according to Fig. 1 B, beyond about $s = 50$ nm. Given the retraction velocity $v = 500$ nm/s in Fig. 2 B, these bonds thus exhibit lifetimes of 0.1 s or more even in the presence of load.

Further, we demonstrated that our force spectroscopy data are in very good agreement with the Bell model (14,23), which is the gold standard for analyzing DFS experiments. It is well known that this model is able to describe very well the loading-rate dependence of the most probable rupture forces, f^*, for most DFS experiments, but it usually fails to describe the entire rupture-force distributions. A crucial test of the assumptions of the model is to check whether the plots of $-v\ln n(f)$ against the force, f, are independent of the pulling speed and thus collapse onto a single curve. We found that both our A-T and our AA-T data indeed show the collapse, which is also a prerequisite for applying the method developed by Dudko et al. to estimate the shape of the reaction potential (19). Based on our experimental data, we found that a parabolic potential well with a cusp barrier, a cubic reaction potential, and a piecewise linear potential are all equally compatible with those data.

Another prerequisite for the Bell model is that the rupture force is related to the breaking of a single molecular bond. Our data are consistent with this model, showing that we indeed observe single-molecule rupture events. As an additional test, we loosened one of our selection criteria in data preprocessing to artificially include some multiple-rupture events. Using the same data set, we were able to demonstrate that the inclusion of such events results in retraction-speed-dependent $-v\ln n(f)$ against the force, f, plots. To quantify the frequency of multiple-rupture events, we generalized the multiple-bond model of Akhremitchev et al. (15). This allowed us to estimate the number of double and triple events.

Our finding that the inclusion of multiple-rupture events leads to an apparent retraction-speed dependence of the $-v\ln n(f)$ against f plots is of particular interest, because it has been shown that a similar behavior could be observed for other reasons, such as random variations and fluctuations of the local molecular environment and orientational fluctuations of the molecular complex relative to the direction of the applied pulling force (26). Thus, rigorous exclusion of the multiple rupture events is required if deviations from the standard Bell model are to be used to learn details of the dissociation pathway.

Finally, we found that inclusion of even a significant amount of nonsingle-rupture events still gives reasonable values for k_{off} and x_b using only the most probable rupture forces in DFS experiments, though, as discussed above, this complicates further analysis of the dissociation pathway. Approaches like the heterogeneous bond model (26) will allow us in the future to get detailed information about the bound complexes that goes well beyond the determination of k_{off} and x_b.

SUPPORTING MATERIAL

REFERENCES

1. Sartorius, J., and H. J. Schneider. 1996. A general scheme based on empirical increments for the prediction of hydrogen-bond associations

of nucleobases and of synthetic host-guest complexes. *Chem. Eur. J.* 2:1446–1452.

2. Englander, S. W., and N. R. Kallenbach. 1983. Hydrogen exchange and structural dynamics of proteins and nucleic acids. *Q. Rev. Biophys.* 16:521–655.

3. Gueron, M., and J. L. Leroy. 1992. Base-pair opening in double-stranded nucleic acids. *In* Nucleic Acids and Molecular Biology. F. Eckstein and D. M. J. Lilley, editors. Springer-Verlag, New York. 1–22.

4. Leroy, J. L., E. Charretier, …, M. Guéron. 1988. Evidence from base-pair kinetics for two types of adenine tract structures in solution: their relation to DNA curvature. *Biochemistry.* 27:8894–8898.

5. Bhattacharya, P. K., J. Cha, and J. K. Barton. 2002. ¹H NMR determination of base-pair lifetimes in oligonucleotides containing single base mismatches. *Nucleic Acids Res.* 30:4740–4750.

6. Rief, M., H. Clausen-Schaumann, and H. E. Gaub. 1999. Sequence-dependent mechanics of single DNA molecules. *Nat. Struct. Biol.* 6:346–349.

7. Clausen-Schaumann, H., M. Rief, …, H. E. Gaub. 2000. Mechanical stability of single DNA molecules. *Biophys. J.* 78:1997–2007.

8. Lee, G. U., L. A. Chrisey, and R. J. Colton. 1994. Direct measurement of the forces between complementary strands of DNA. *Science.* 266:771–773.

9. Sattin, B. D., A. E. Pelling, and M. C. Goh. 2004. DNA base pair resolution by single molecule force spectroscopy. *Nucleic Acids Res.* 32:4876–4883.

10. Saenger, W. 1984. Principles of Nucleic Acid Structure. Springer-Verlag, New York.

11. Huang, S., J. He, …, S. Lindsay. 2010. Identifying single bases in a DNA oligomer with electron tunnelling. *Nat. Nanotechnol.* 5:868–873.

12. Zlatanova, J., S. M. Lindsay, and S. H. Leuba. 2000. Single molecule force spectroscopy in biology using the atomic force microscope. *Prog. Biophys. Mol. Biol.* 74:37–61.

13. Fuhrmann, A., and R. Ros. 2010. Single-molecule force spectroscopy: a method for quantitative analysis of ligand-receptor interactions. *Nanomedicine (Lond).* 5:657–666.

14. Evans, E., and K. Ritchie. 1997. Dynamic strength of molecular adhesion bonds. *Biophys. J.* 72:1541–1555.

15. Guo, S., C. Ray, …, B. B. Akhremitchev. 2008. Effects of multiple-bond ruptures on kinetic parameters extracted from force spectroscopy measurements: revisiting biotin-streptavidin interactions. *Biophys. J.* 95:3964–3976.

16. He, J., L. Lin, …, S. Lindsay. 2007. Identification of DNA basepairing via tunnel-current decay. *Nano Lett.* 7:3854–3858.

17. Fuhrmann, A., D. Anselmetti, …, P. Reimann. 2008. Refined procedure of evaluating experimental single-molecule force spectroscopy data. *Phys. Rev. E.* 77:031912.

18. Getfert, S., M. Evstigneev, and P. Reimann. 2009. Single-molecule force spectroscopy: practical limitations beyond Bell's model. *Physica A.* 388:1120–1132.

19. Dudko, O. K., G. Hummer, and A. Szabo. 2006. Intrinsic rates and activation free energies from single-molecule pulling experiments. *Phys. Rev. Lett.* 96:108101.

20. Raible, M., M. Evstigneev, …, R. Ros. 2004. Theoretical analysis of dynamic force spectroscopy experiments on ligand-receptor complexes. *J. Biotechnol.* 112:13–23.

21. Ray, C., J. R. Brown, and B. B. Akhremitchev. 2007. Rupture force analysis and the associated systematic errors in force spectroscopy by AFM. *Langmuir.* 23:6076–6083.

22. Hummer, G., and A. Szabo. 2003. Kinetics from nonequilibrium single-molecule pulling experiments. *Biophys. J.* 85:5–15.

23. Bell, G. I. 1978. Models for the specific adhesion of cells to cells. *Science.* 200:618–627.

24. Smith, S. B., Y. Cui, and C. Bustamante. 1996. Overstretching B-DNA: the elastic response of individual double-stranded and single-stranded DNA molecules. *Science.* 271:795–799.

25. Imparato, A., and L. Peliti. 2004. Kinetic barriers in RNA unzipping. *Eur. Phys. J. B.* 39:357–363.

26. Raible, M., M. Evstigneev, …, P. Reimann. 2006. Theoretical analysis of single-molecule force spectroscopy experiments: heterogeneity of chemical bonds. *Biophys. J.* 90:3851–3864.

27. Fuhrmann, A., J. C. Schoening, …, R. Ros. 2009. Quantitative analysis of single-molecule RNA-protein interaction. *Biophys. J.* 96:5030–5039.

28. Kaur, P., A. Qiang-Fu, …, S. Lindsay. 2011. Antibody-unfolding and metastable-state binding in force spectroscopy and recognition imaging. *Biophys. J.* 100:243–250.

29. Hinterdorfer, P., W. Baumgartner, …, H. Schindler. 1996. Detection and localization of individual antibody-antigen recognition events by atomic force microscopy. *Proc. Natl. Acad. Sci. USA.* 93:3477–3481.

30. Ros, R., F. Schwesinger, …, L. Tiefenauer. 1998. Antigen binding forces of individually addressed single-chain Fv antibody molecules. *Proc. Natl. Acad. Sci. USA.* 95:7402–7405.

31. Oesterhelt, F., M. Rief, and H. E. Gaub. 1999. Single molecule force spectroscopy by AFM indicates helical structure of poly(ethylene-glycol) in water. *N. J. Phys.* 1 6.1–6.11.

32. Sulchek, T., R. W. Friddle, and A. Noy. 2006. Strength of multiple parallel biological bonds. *Biophys. J.* 90:4686–4691.

33. Strunz, T., K. Oroszlan, …, H. J. Güntherodt. 1999. Dynamic force spectroscopy of single DNA molecules. *Proc. Natl. Acad. Sci. USA.* 96:11277–11282.

34. Ke, C., M. Humeniuk, …, P. E. Marszalek. 2007. Direct measurements of base stacking interactions in DNA by single-molecule atomic-force spectroscopy. *Phys. Rev. Lett.* 99:018302.

35. Krautbauer, R., M. Rief, and H. E. Gaub. 2003. Unzipping DNA oligomers. *Nano Lett.* 3:493–496.

36. Diezemann, G., and A. Janshoff. 2008. Dynamic force spectroscopy: analysis of reversible bond-breaking dynamics. *J. Chem. Phys.* 129:084904.

37. Zou, S., H. Schönherr, and G. J. Vancso. 2005. Stretching and rupturing individual supramolecular polymer chains by AFM. *Angew. Chem. Int. Ed. Engl.* 44:956–959.

38. Zou, S., H. Schönherr, and G. J. Vancso. 2005. Force spectroscopy of quadruple H-bonded dimers by AFM: dynamic bond rupture and molecular time-temperature superposition. *J. Am. Chem. Soc.* 127:11230–11231.

39. Dudko, O. K., J. Mathé, …, G. Hummer. 2007. Extracting kinetics from single-molecule force spectroscopy: nanopore unzipping of DNA hairpins. *Biophys. J.* 92:4188–4195.

40. Husson, J., and F. Pincet. 2008. Analyzing single-bond experiments: influence of the shape of the energy landscape and universal law between the width, depth, and force spectrum of the bond. *Phys. Rev. E.* 77:026108.

41. Bartels, F. W., B. Baumgarth, …, A. Becker. 2003. Specific binding of the regulatory protein ExpG to promoter regions of the galactoglucan biosynthesis gene cluster of *Sinorhizobium meliloti*—a combined molecular biology and force spectroscopy investigation. *J. Struct. Biol.* 143:145–152.

42. Eckel, R., R. Ros, …, D. Anselmetti. 2005. Supramolecular chemistry at the single-molecule level. *Angew. Chem. Int. Ed. Engl.* 44:484–488.

43. Schwesinger, F., R. Ros, …, A. Pluckthun. 2000. Unbinding forces of single antibody-antigen complexes correlate with their thermal dissociation rates. *Proc. Natl. Acad. Sci. USA.* 97:9972–9977.

44. Morfill, J., K. Blank, …, H. E. Gaub. 2007. Affinity-matured recombinant antibody fragments analyzed by single-molecule force spectroscopy. *Biophys. J.* 93:3583–3590.

45. Kienberger, F., G. Kada, …, P. Hinterdorfer. 2000. Recognition force spectroscopy studies of the NTA-His⁶ bond. *Single Molecules.* 1:59–65.

46. Bartels, F. W., M. McIntosh, …, A. Becker. 2007. Effector-stimulated single molecule protein-DNA interactions of a quorum-sensing system in *Sinorhizobium meliloti. Biophys. J.* 92:4391–4400.

47. Bonanni, B., A. S. M. Kamruzzahan, …, S. Cannistraro. 2005. Single molecule recognition between cytochrome *c* 551 and gold-immobilized azurin by force spectroscopy. *Biophys. J.* 89:2783–2791.

48. Karácsony, O., and B. B. Akhremitchev. 2011. On the detection of single bond ruptures in dynamic force spectroscopy by AFM. *Langmuir.* 27:11287–11291.

49. Getfert, S., and P. Reimann. 2012. Hidden multiple bond effects in dynamic force spectroscopy. *Biophys. J.* 102:1184–1193.